remote sensing

MDPI

Article

Mapping Forest Cover and Forest Cover Change with Airborne S-Band Radar

Ramesh K. Ningthoujam [1,*], Kevin Tansey [1,†], Heiko Balzter [1,2,†], Keith Morrison [3], Sarah C. M. Johnson [1], France Gerard [4], Charles George [4], Geoff Burbidge [5], Sam Doody [5], Nick Veck [6], Gary M. Llewellyn [7] and Thomas Blythe [8]

1 Department of Geography, Centre for Landscape and Climate Research, University of Leicester, Leicester LE1 7RH, UK; kjt7@le.ac.uk (K.T.); hb91@le.ac.uk (H.B.); sj239@le.ac.uk (S.C.M.J.)
2 National Centre for Earth Observation, University of Leicester, Leicester LE1 7RH, UK
3 Radar Group, School of Cranfield Defence And Security, Cranfield University, Shrivenham, Swindon SN6 8LA, UK; k.morrison@cranfield.ac.uk
4 Centre for Ecology & Hydrology, Wallingford OX10 8BB, UK; ffg@ceh.ac.uk (F.G.); ctg@ceh.ac.uk (C.G.)
5 Airbus Defence and Space–Space Systems, Anchorage Road, Portsmouth, Hampshire PO3 5PU, UK; geoff.burbidge@airbus.com (G.B.); sam.doody@airbus.com (S.D.)
6 Satellite Applications Catapult, Electron Building Fermi Avenue Harwell, Oxford Didcot, Oxfordshire OX11 0QR, UK; Nick.Veck@sa.catapult.org.uk
7 Natural Environment Research Council Airborne Research & Survey Facility, Firfax Building, Meteor Business Park, Cheltenham Road East, Gloucester GL2 9QL, UK; gaew@nerc.ac.uk
8 Forestry Commission, Bristol and Savernake, Leigh Woods Office, Abbots Leigh Road, Bristol BS8 3QB, UK; Thomas.Blythe@forestry.gsi.gov.uk
* Correspondence: rkn8@le.ac.uk or rningthoujam@sky.com; Tel.: +44-116-252-3820
† These authors contributed equally to this work.

Academic Editors: Sangram Ganguly, Nicolas Baghdadi and Prasad S. Thenkabail
Received: 11 April 2016; Accepted: 4 July 2016; Published: 8 July 2016

Abstract: Assessments of forest cover, forest carbon stocks and carbon emissions from deforestation and degradation are increasingly important components of sustainable resource management, for combating biodiversity loss and in climate mitigation policies. Satellite remote sensing provides the only means for mapping global forest cover regularly. However, forest classification with optical data is limited by its insensitivity to three-dimensional canopy structure and cloud cover obscuring many forest regions. Synthetic Aperture Radar (SAR) sensors are increasingly being used to mitigate these problems, mainly in the L-, C- and X-band domains of the electromagnetic spectrum. S-band has not been systematically studied for this purpose. In anticipation of the British built NovaSAR-S satellite mission, this study evaluates the benefits of polarimetric S-band SAR for forest characterisation. The Michigan Microwave Canopy Scattering (MIMICS-I) radiative transfer model is utilised to understand the scattering mechanisms in forest canopies at S-band. The MIMICS-I model reveals strong S-band backscatter sensitivity to the forest canopy in comparison to soil characteristics across all polarisations and incidence angles. Airborne S-band SAR imagery over the temperate mixed forest of Savernake Forest in southern England is analysed for its information content. Based on the modelling results, S-band HH- and VV-polarisation radar backscatter and the Radar Forest Degradation Index (RFDI) are used in a forest/non-forest Maximum Likelihood classification at a spatial resolution of 6 m (70% overall accuracy, $\kappa = 0.41$) and 20 m (63% overall accuracy, $\kappa = 0.27$). The conclusion is that S-band SAR such as from NovaSAR-S is likely to be suitable for monitoring forest cover and its changes.

Keywords: forest/non-forest; forest cover change; S-band SAR; MIMICS-I model; Savernake forest

1. Introduction

1.1. Remote Sensing and Forest Mapping

Forests play a pivotal role in biogeophysical feedbacks of the terrestrial biosphere with the climate system [1] and constitute one of the main components of the global carbon cycle [2] in the form of woody aboveground biomass (AGB) [3]. Availability of information on forest cover and accurate mapping algorithm are essential for monitoring and managing forests [4]. Accuracies of forest cover information vary depending on the type of tools and methods used. For example, the United Nation's Food and Agriculture Organization (FAO), has provided estimates of global forest cover at 5–10 year intervals since 1946 based on national statistics [5], largely relying on forest inventory data, models and expert opinion. However, there is a lack of consistency in terms of defining forest and assessment methods of different countries [6]. Moreover, there are data gaps in national forest inventories in many parts of the world, particularly areas with inaccessible problems. To overcome these uncertainties on forest cover extent, surveys based on remote sensing are now being used operationally [7].

For a consistent and systematic study on global monitoring of forested areas, use of Earth observation data from satellite offers robust and continuous data with large area coverage and repetitive observations [8] and can reduce the cost and time of field inventories. At the small scale, remote sensing also provides forest maps on inventory estimates with precision for limited field data and can be used for purposes related to timber production, procurement and ecological studies [9]. Therefore, remotely sensed data have been incorporated into operational forest inventories. Over the past decades, different forest cover maps at continental to global scales have been generated utilising optical sensors with fine, medium and coarse spatial resolutions [4,10–12]. The majority of the optical-derived forest/non-forest (F/NF) maps have been generated from optical data acquired in a single year or period due to persistent cloud cover using time-series composite data. Additionally, they have been used for mapping forest cover and AGB of forest where relatively simple stand structure and gradients of cover exists such as wooded savannas [13].

For the first time, forest cover maps with the annual forest gain and loss from 2000 to 2012 have been produced using multi-temporal fine-resolution Landsat data at global scale [4]. The existing optical-derived global maps showing areas of F/NF reveal differences in the forested area estimations ranging from 3.5 billion ha to 4 billion ha primarily due to the varying definition of forest and methodologies. In general, forest is defined as all contiguous area >0.5 ha with at least 10% canopy cover and 2–5 m height [5]. Moreover, the spectral reflectances (both absorbed and scattered) of forest canopy components (leaves, needles and branches) at optical wavelengths are sensitive to weather conditions and closely related to two-dimensional structure (i.e., amount of foliage cover, leaf area index) and their biochemical properties such as chlorophyll, nitrogen, lignin and cellulose content and the difficulty in separating mixed vegetation types has resulted in varying accuracies between 66.9% (IGBP DISCover 1.1 km) and 78.3% (MODIS 1 km) at global scale [14]. Information related to radiation scattering from leaves, branches, trunks (i.e., forest structure particularly height) and the ground is highly desirable for differentiating woody from herbaceous or other mixed vegetation where the use of optical data is often problematic. Specific information related to stands of different species, age or density [15] including stand information with tree trunk diameter and stem volume [16] will aid in classification of forest cover types. Forest structural properties related to crown architecture at tree level and spatial heterogeneity distribution at stand level will also be useful in forest cover mapping [15].

1.2. Forest/Non-Forest Mapping Using SAR

Approximately 47% of the Earth's land surface was assumed to be covered by closed forest about 8000 years ago based on numerous global and regional biogeographic information [17]. Since the last decades, nearly 30% of the world's land area is forested due to wildfires, drought, logging and large-scale deforestation particularly in the tropics [18]. Within this area, different forest types occur

based on climatic (global), soil, topography and disturbance factors at landscape level [19]. They also constitute about 80% of terrestrial AGB as a function of forest growth (e.g., regeneration) and mortality (e.g., logging, deforestation) [18]. The extent of progressive losses in forest area and forest biomass (productivity) caused by human activities has been substantial, resulting in significant greenhouse gas emissions and regional to global climate changes and carbon budgets [20]. Therefore, accurate measurement of the forested areas and spatio-temporal variations in the biomass of these forests at local, national to global scales is needed.

For an operational forest cover monitoring system at high spatial and temporal resolutions, Synthetic Aperture Radar (SAR) systems have emerged as robust tools which can penetrate clouds and record signals which originate from scattering within the vertical canopy layer [21,22]. For example, Shimada, Itoh, Motohka, Watanabe, Shiraishi, Thapa and Lucas [22] have generated global F/NF cover maps (2007–2010) at 25 m resolution from the Advanced Land Observing Satellite (ALOS) Phased Arrayed L-band Synthetic Aperture Radar (PALSAR) HV gamma-nought (γ^0) reporting around 85% overall accuracy. For the past three decades, significant efforts in microwave remote sensing have been devoted to interpreting the radar backscatter [23] for improved forest classification accuracy [24] and biophysical retrievals [25,26]. For information related to forest attributes at the stand level such as cleared-felled or canopy degradation, S-band radar data at 6 m resolution from NovaSAR-S could potentially provide a more useful data product than is currently available from Sentinel-1, ALOS-2 and other SAR sensors that provide global coverage.

Understanding the relationships between SAR backscatter at different wavelengths and polarisation combinations and forest canopy parameters is critically important for developing forest monitoring methods. However, the sensitivity of the radar backscatter to different canopy elements (leaves, branches and trunks) cannot easily be quantified based on image data alone (without complementary field data) due to the inter-relationship between forest parameters and radar parameters. Simulations from microwave canopy radiative transfer models provide insight into the complex interactions of the radar wave with the different components of the canopy as a function of wavelength, incidence angle and polarisations [26–29]; for instance, increasing level of penetration with increasing wavelength. Such models have shown that the low frequencies (P- and L-band), in particular co-polarized (horizontal transmit and horizontal receive—HH, vertical transmit and vertical receive—VV) channels produce stronger scattering from larger scattering elements (branches, trunks) with high frequencies (X- and C-band) from leaves and needles. This can be understood by radar being most sensitive to features in a scene with dimensions characteristic of the scale of the probing wavelength, combined with increasing canopy penetration wave with increasing wavelength. In contrast to X-, C-, L- and P-band, the nature of the S-band microwave scattering mechanism in forest canopies is poorly studied to date due to the historic lack of availability of S-band SAR data. The S-band (3.1–3.3 GHz) lies between the longer L-band (1–2 GHz) and the shorter C-band (5–6 GHz).

1.3. Potential of S-Band Data for Forest Mapping

The first S-band SAR observations from space were provided by the Russian Almaz-1 satellite, which carried a single-polarized HH S-band SAR sensor operating between 1991 and 1992. Since the Almaz-1 mission, interest in S-band SAR has led to the launch of the Environment and Disaster Monitoring Satellite Huan Jing -1 Constellation (HJ-1C) from China [30] and new S-band SAR missions are planned, e.g., the UK NovaSAR S-band [31] and the joint NASA-ISRO Synthetic Aperture Radar (NISAR) missions [32]. NovaSAR is planned to provide S-band data with StripMap and ScanSAR resolution modes at 6 m and 20 m respectively.

Few published studies have investigated S-band radar responses to agricultural crops and forest canopies to date. The sensitivity of S-band backscatter to maize crops was dominantly volume scattering due to the random distribution over the whole plants [33]. The Michigan Microwave Canopy Scattering (MIMICS) model suggests that S-band backscatter is sensitive to the temporal dynamics of the structure of wheat crops [34]. In the young fir, S-band backscatter arises from the

needles and branches resulting in lower volume scattering due to the conical structure of conifer species [35]. The capability of S-band backscatter to map agricultural crop canopies [36] and forested areas [37] using an integration of polarimetric scattering entropy H/average alpha angle α and Pauli's decomposition techniques and salt marsh habitat mapping using a Random Forest algorithm [38] have also been explored using airborne very-high resolution S-band data. Studies by Yatabe and Leckie [39] and Fransson, et al. [40] have demonstrated the mapping of clear-felled and forested areas using S-band Almaz-1 in boreal forest of Canada and Sweden.

The fine 6 m resolution data from NovaSAR could provide a useful and better than other available datasets from Sentinel-1, ALOS-2 and other SAR sensors that provide global coverage. This means that the radar pulse at this frequency can provide the information in relation to the small-scale changes in the forest ecosystem particularly degraded and disturbed areas due to its sensitivities to the forest canopy and its structural components. Modelling studies have highlighted the sensitivity of longer wavelength at L-band to the varying sizes of branch canopy and canopy density [29] and similar sensitivity to varying canopy density, branching level and branch size have also been found to be sensitive to S-band radar pulse.

The main objective of this study is to classify S-band radar backscatter data to produce F/NF cover and change maps using a Maximum Likelihood Classification (MLC) algorithm at different spatial resolutions that match the anticipated acquisition modes of NovaSAR-S. Scattering mechanisms in the canopy and from the ground have been investigated from radiative transfer modelling experiment with MIMICS-I [29]. This paper is organised as follows: Section 2 gives the details of test site, the dataset involved in the study and the used methodology. Section 3 mainly deals with the results and discussion and the conclusions are drawn in Section 4.

2. Experimental Section

2.1. Site Description

Savernake forest (51°23'13"N, 1°43'19"W) is located near Marlborough in England, UK (Figure 1). The study site of Savernake forest was chosen based on its diverse land cover types. A field campaign was carried out to collect ground data. The forest is composed of mixed stands of temperate deciduous and coniferous species with varying tree densities, canopy height, growing stock, and age class. Main deciduous species include ancient beech (*Fagus sylvatica*), birch (*Betula pendula*) and oak (*Quercus* spp.) with mixed species of yew, ash, common lime, crab apple, elm, field maple, hazel, horse chestnut etc. Dominant coniferous species consist of Scots pine (*Pinus sylvestris*), Corsican pine (*Pinus nigra*), Norway spruce (*Picea abies*) and Western hemlock (*Tsuga heterophylla*). The non-forest comprises three main land cover classes, as grassland, clear-felled areas and bare-ground. The existence of mix forest/non-forest classes in the study site could potentially lead to lower accuracy level and confusion in any classification algorithm.

Savernake forest is maintained by the Forestry Commission (FC) and the forest is divided for management purposes into sub-compartments of 4 ha average size. A series of management operations have been undertaken in Savernake forest between December 2012 and July 2013. For example, two sub-compartments of sizes 3.45 ha and 5.2 ha have been completely clear-felled followed by plantation with Douglas fir and oak seedlings. Otherwise, most of the sub-compartments were subject to thinning operations to enhance timber production. Topography is relatively flat with an average elevation of 107 m and 1% slope with a south-eastern aspect [41]. The forest receives an average of 750 mm of annual precipitation and has an average annual temperature of 11.3 °C. Geologically, the parent soil material is characterized by Jurassic Clay (Oxford) with Eutric vertisol, and has a soil pH of 3.9–6.2.

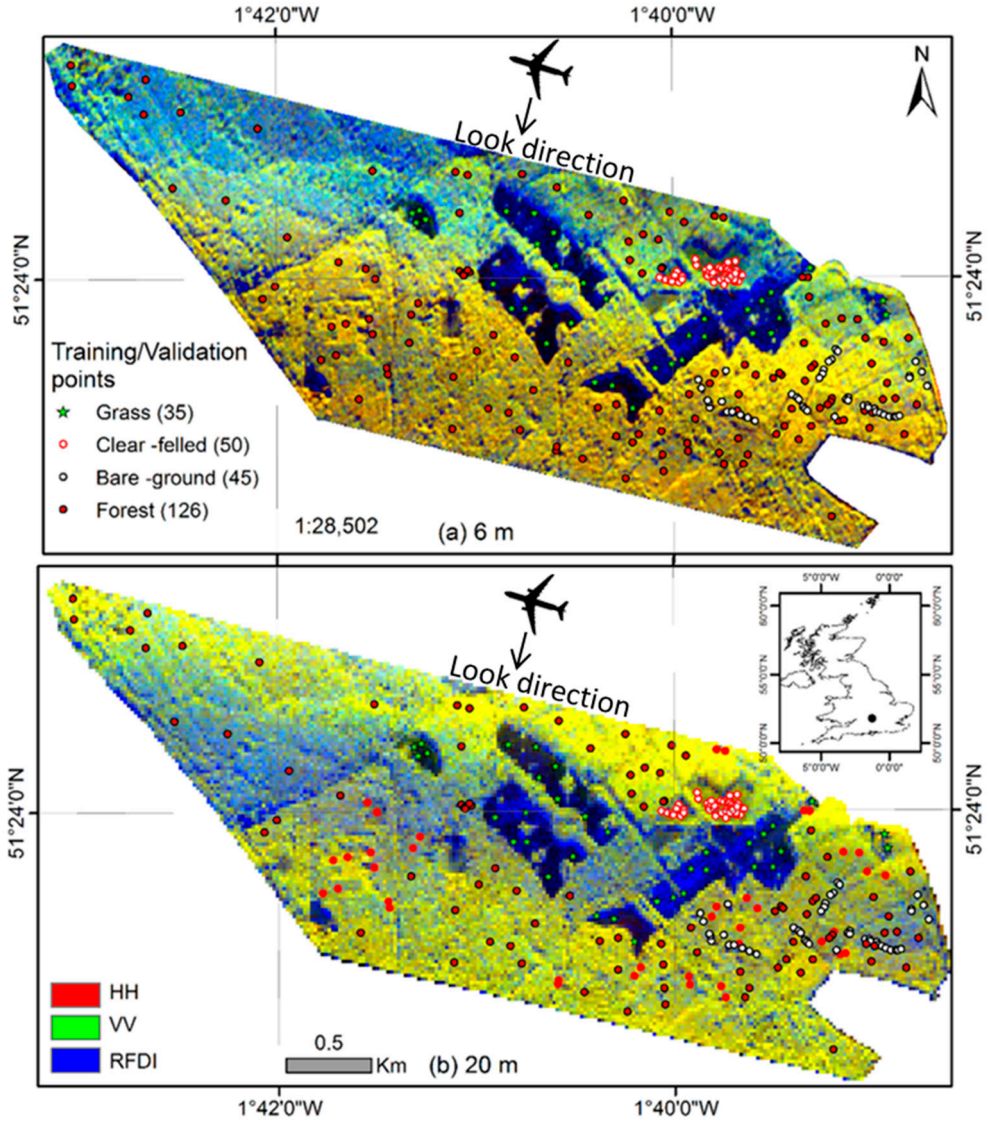


Figure 1. Field, Forestry Commission Geographical Information System (FC GIS), ancient tree plot locations for 126 forest and 130 non-forest (training and validation plots) overlaid on 2014 acquired S-band FCC at 6 m (**a**) and 20 m; (**b**) pixel resolutions for Savernake Forest.

2.2. SAR Data and Processing

A number of SAR airborne campaigns have been undertaken in Europe to investigate the capabilities of different SAR sensors to forest characteristics. For example, the MAESTRO-I campaign during August 1989 utilising the NASA-JPL AIRSAR sensor in four European test sites [28,42] focusing on SAR bands at P-, L-, C- and X-frequencies. Now, for the first time, extensive S-band SAR campaign have been conducted over the temperate region of UK known as the 'AirSAR Campaign' in 2010 and 2014. The Airborne SAR Demonstrator Facility 'AirSAR' is a collaborative project operated by Airbus Defence and Space (UK) with the Natural Environment Research Council (NERC) and the Satellite Applications Catapult [43].

The frequency band used in the study is S-band (3.1–3.3 GHz) with a swath width of 1.92 km and incidence angles from 16° to 42.5°. The Single-Look Complex (SLC) imagery is provided with 0.75 m pixel in both ground and cross-range spacing with 4.48 looks in azimuth and 1 look in range direction [43]. Their characteristics are summarized in Table 1.

Table 1. Summary of S-band AirSAR images used in this research. SLC = Single-Look Complex.

Site	Acquisition Date	Incidence Angles (°)	Polarisation	SLC Pixel Size (m)
Savernake	16 June 2010	22–39.9	Quad	0.75
Savernake	24 June 2014	16–42.5	Quad	0.75

An antenna pattern correction with polynomials of different order was applied, and the 5th order polynomial provided the best fit. To reduce the speckle, conversion of the SLC imagery into multi-look complex images using a 5 × 5 kernel corresponding to 3.75 m pixel size resolution was performed. Further image processing was carried out with seven different adaptive filters using 3 × 3, 5 × 5 and 7 × 7 kernels where Enhanced Frost filter performed best for reducing speckle with a 5 × 5 kernel. These include Kuan, Lee, Enhanced Lee, Frost, Enhanced Frost, Gamma and Local Sigma filters. The analysis was based on the mean and standard deviation (SD) of the DN values on the assumption that the filter that retains the mean of the DN values of the raw data while reducing the SD to the minimum, is the ideal filter for reducing the speckle effect. For all the polarisations and in different kernels (3, 5, 7), the Enhanced Frost, Enhanced Lee, Local Sigma and Kuan filters produce similar mean values to the raw data. However, the SD increases from Enhanced Frost up to Kuan filters. Frost, Gamma and Lee filters produces maximum mean values and highest SD relative to the unfiltered raw data. Figure 2 represents the performance of different filters for reducing the SAR speckle with HV polarisation (2014 data).

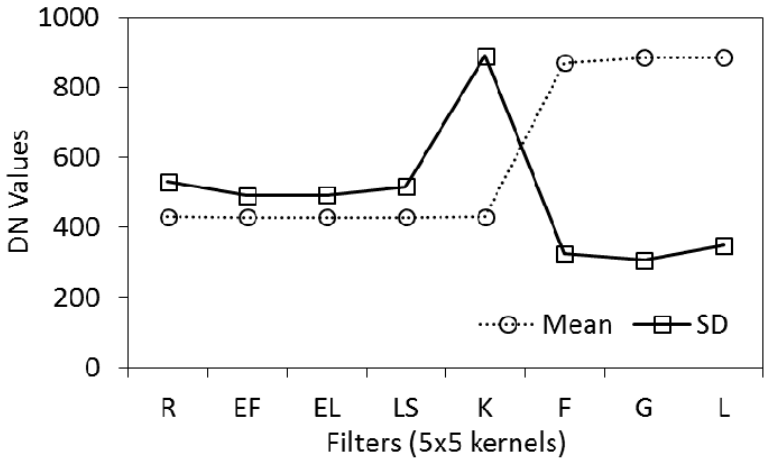


Figure 2. The effects of different adaptive filters on HV polarised channel at 5 × 5 kernel (R–unfiltered raw, EF–Enhanced Frost, EL–Enhanced Lee, LS–Local Sigma, K–Kuan, F–Frost, G–Gamma and L-Lee).

As the study area has only a minimal topographic slope, geo-coding of the SAR imagery was done using an Ordnance Survey map (Projection: United Kingdom, Datum: Ordnance Survey of Great Britain–OSGB 1936) as reference with 30 widely distributed ground control points (GCPs), a second-order polynomial and nearest neighbour re-sampling to 6 m and 20 m pixel resolution achieving a root mean square error (RMSE) of half a pixel. For the absolute radiometric calibration of the airborne demonstrator data, corner reflectors were placed in the near, centre and far range of the swath with corresponding incidence angles of 22.11°, 30.38° and 39.96°. The radar backscatter coefficient was calculated using Equation (1) according to an Airbus Defence and Space technical report [44]:

$$[\sigma^0 = 10 \log_{10}(DN^2) - Kcal] \quad (1)$$

where: σ^0 = radar backscatter (dB), DN = pixel amplitude and Kcal = calibration constant. The calibration constants for Savernake forest are 71.5 dB for HH and VH, and 71.47 dB for VV

and HV polarisations for the image acquired on 16 June 2010, and 71.8 dB for HH, VH and 72.62 dB for VV and HV polarisations for the image acquired on 24 June 2014.

To implement forest cover change detection, a multi-temporal image calibration (or normalization) of the 2010 and 2014 data was performed to ensure absolute radiometric calibration [45]. This was done by re-calibrating 2010 data based on 2014 data using the basic statistics (minimum, maximum, mean DN values) of all polarisations from all land cover types. The maximum DN values were 3398, 6601 and 1530 in 16 June 2010 and 24,356, 32,658 and 5040 in 24 June 2014 for HH, VV and HV polarisations. Therefore, correction factors of 7.16, 4.94 and 3.29 for HH, VV and HV polarisations were applied to 16 June 2010 to match the intensity of 24 June 2014 data. This is being verified by linear regression models based on 2640 known tree targets from the ancient tree database based on corrected 2010 and original 2014 data (Figure 3).

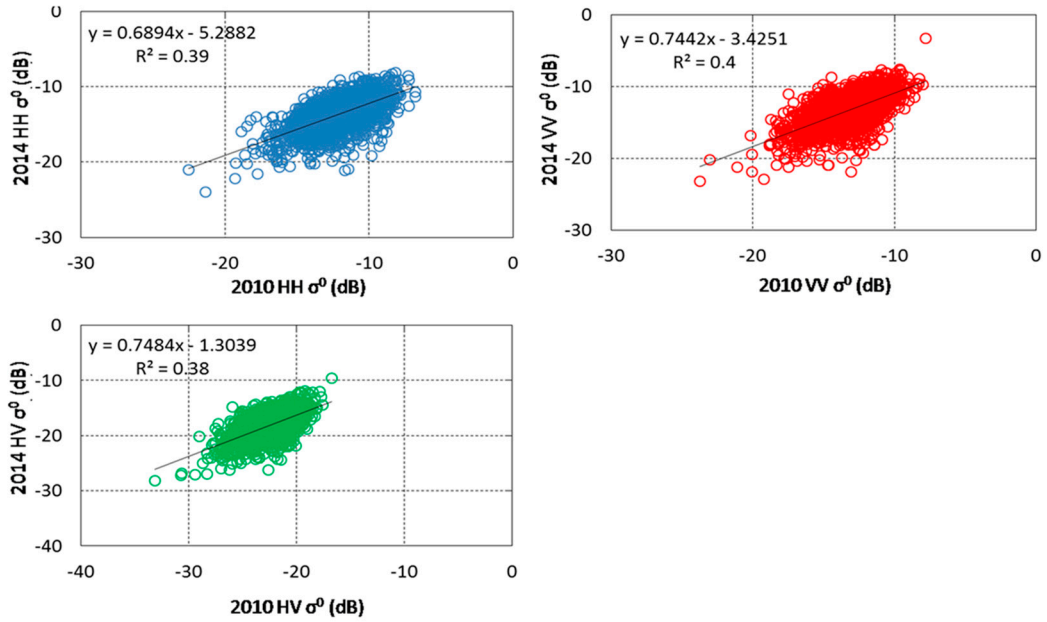


Figure 3. S-band backscatter comparison for forest (2640 tree points) class between re-scaled 2010 and 2014 synthetic aperture radar (SAR) imageries.

2.3. Ancillary Data

The Forestry Commission Geographical Information System (FC GIS) database is a spatially comprehensive vector database of forest type, species, planting year, planting density and yield class for each forest stand. This database contains 215 sub-compartments for Savernake forest. The digital sub-compartment data were projected to the United Kingdom projection of the SAR image data with OSGB 1936. Information on forest type and tree species is used to train the MLC algorithm. Additionally, the ancient tree database contains approximately 2640 point locations within the image area. Each point contains detailed attribute information including diameter at breast height (DBH), canopy height (H) and tree species having a maximum tree DBH of 350 cm and canopy height of 35 m. In August 2012 and March 2015, a total of 70 sample plots were surveyed in the field, with two circular sample areas of 20 m diameter each of 35 sub-compartments with different tree species of both deciduous and coniferous forest types.

2.4. S-Band Radar Scattering Characteristics in Forest/Non-Forest Areas

This study uses the radiative transfer model MIMICS-I [29] as a tool for investigating S-band backscatter predictions and dominant scattering from forest canopies. The input parameters for MIMICS-I can be divided into two major classes related to: (1) microwave characteristics (polarisation

and incidence angle); and (2) physical descriptions of the canopy (layers of leaves, needles, branches and trunk) as well as soil properties (soil moisture content and surface roughness). MIMICS-I model describes the vegetation layer as canopy and trunk layers where different layers of branches (viz., primary to sixth branch level) with different sizes are considered.

Forest biophysical parameters were assumed to have remained unchanged between the 2010 and 2014. Therefore, tree density, stem diameter at breast height, canopy height and branch size were assumed constant. A small number of model parameters need to be adjusted for the different imaging conditions of the two sets of radar observations in 2010 and 2014, namely soil moisture content and structure of the stands. The soil moisture information was derived from Wytham Woods test site within the AirSAR campaign, being collected by the Centre for Ecology and Hydrology in 23 June 2014. Different percentages of soil components for sand, silt and clay were derived from 1 km soil data set of Batjes [46]. Ground measurements such as density of leaves, needles and branches including their spatial orientation are extremely difficult to obtain and were not available for this site. Therefore, an informed estimate based on the literature is assumed for such structural canopy parameters. All the estimated values are derived from the MIMICS-I model technical report [47]. A list of input parameters used in the MIMICS simulations is given in Table 2. The sensitivity of S-band radar backscatter to forest canopy properties and soil characteristics was investigated as a function of polarisation and incidence angle. For this study in context to forest/non-forest assessment, only the total backscatter return from forest canopy (up to secondary branch levels) and soil properties were assessed and reported. Details related to the canopy transmissivity and contribution of the individual interactions to the total canopy backscatter at S-band will be reported in a companion paper by Ningthoujam et al., (accepted).

Table 2. Numerical values of input parameters for MIMICS-I model: bold = estimated; normal = measured.

Parameter	Deciduous (Birch)	Coniferous (Norway Spruce)
Trunk layer		
Height (m)	8	8, 16
Diameter (m)	2.4	2.08
Canopy density (m^{-2})	0.11	0.2, 0.1, 0.05
Moisture (gravimetric)	**0.5**	**0.6**
Crown layer		
Crown thickness (m)	**1, 2, 3, . . . , 10**	**11**
Leaf/needle density (m^{-3})	**100, . . . , 2000**	**5000, . . . , 100,000**
Leaf/needle moisture (gravimetric)	**0.8**	**0.8**
Leaf Area Index (single-sided)	**5**	**11.9**
Branch density (Primary, Secondary, 3rd, 4th) (m^{-3})	4.1, 0.04, 0.45, 0.37	3.4
Branch length (Primary, Secondary, 3rd, 4th) (m)	0.75, 1.15, 0.52, 0.33	2.0
Branch diameter (Primary, Secondary, 3rd, 4th) (cm)	0.7, 1.6, 0.9, 0.57	2.0
Branch Moisture	**0.4**	**0.6**
Soil root mean square height (cm)	**0.45, 1, 2, 3, 4, 5**	**0.45**
Soil Correlation length (cm)	**18.75**	**18.75**
Soil moisture (volumetric)	0.15–0.5	0.15–0.5
Soil Sand (%)	53	53
Soil Silt (%)	28	28
Soil Clay (%)	19	19
Leaf/needle/branch orientation	**uniform**	**uniform**
dielectric constant (trunk, branch)	**0.4**	**0.6**
Dielectric constant (Leaf)	**0.8**	**0.8**

2.5. Forest Cover Classification

In the first classification approach, only forest and non-forest are defined as the main land cover classes (Figure 4). The ratio between HH- and HV-backscatter was calculated and utilised for the classification. It is also known as the 'Radar Forest Degradation Index' (RFDI) because HH backscatter

is sensitive to both volume and double-bounce scattering while HV backscatter is mostly sensitive to volume scattering from forest canopies [48]. In the second classification approach, non-forest class was classified further into three classes (grassland, clear-felled areas and bare-ground). The definitions and interpretation guidelines used in this methodology are given in Table 3. These classes of non-forest and forest are defined based on the field sample plots and FC GIS data points and are used for training the classification algorithm.

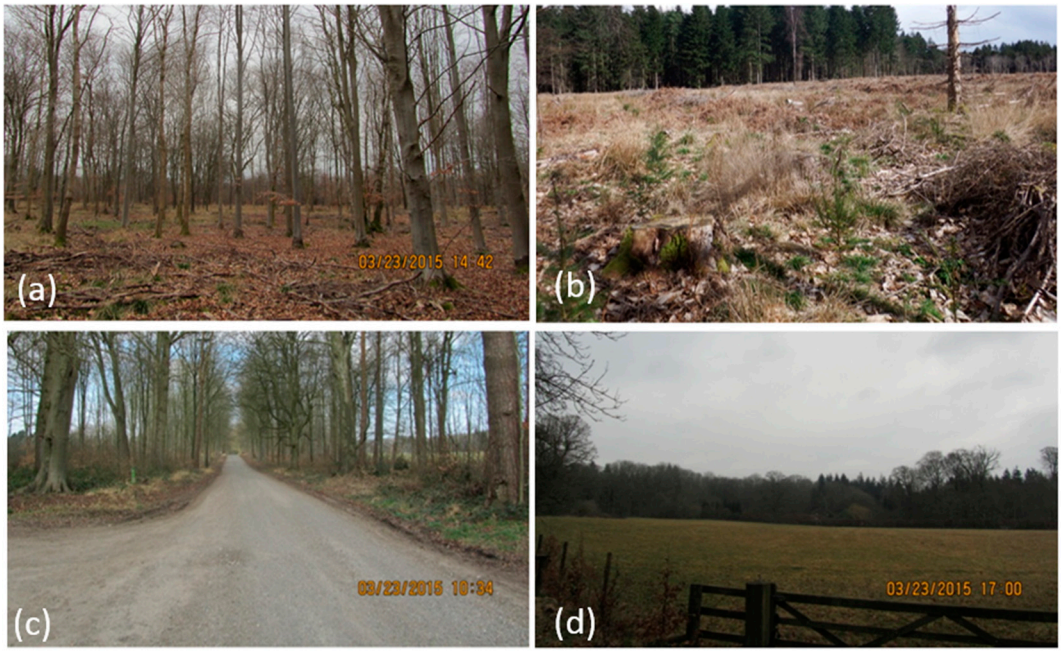


Figure 4. Field photos for deciduous forest (**a**); clear-felled (**b**); bare-ground; (**c**) and grassland; (**d**) at Savernake site (23 March 2015).

Table 3. Definition of forest and non-forest classes.

Class	Definition
Forest	Land dominated by deciduous, conifer and mixed trees with canopy height ⩾3 m, >20 years old and at least 50 tonnes/ha of aboveground biomass.
Grassland	Land dominated by non-woody annual vegetation less than 1 m in height.
Clear-felled	Open area previously occupied by forest due to stand-replacement disturbance. The area is composed of left-over dry leaves, branches and grasses with few dead stumps. This took place between December 2012 and July 2013 in few sub-compartments and planted with Norway spruce and oak seedlings.
Bare-ground	Land surface without any vegetation. This class includes natural and artificial bare surfaces e.g., bare soil, roads and pathways between sub-compartments in the forest.

Prior to the classification, the different scattering behaviour from forest and non-forest stands at S-band was examined for all polarisations. From the backscatter histograms of the forest and non-forest classes, a bimodal shape of the distributions was observed for all polarisations. The S-band scattering behaviour for all polarisations for the F and NF stands based on training sample points of FC sub-compartments is shown in Figure 1. Figure 5 shows box-plots illustrating the backscatter returns at all polarisations in 105 forest and 105 non-forest plots, including different non-forest classes with the training plot locations depicted in Figure 1. Stronger backscattering was recorded by the radar sensor from forested areas in comparison to non-forested ones. HH- and HV-polarisation are best at discriminating F from NF. The VV-backscatter coefficient is highest amongst all polarisations

in both forest and non-forest classes. To further compare with the MIMICS-I simulated backscatter, SAR backscatter across the radar incidence range between 15° to 45° covering both forest types and bare-ground were extracted and analysed.

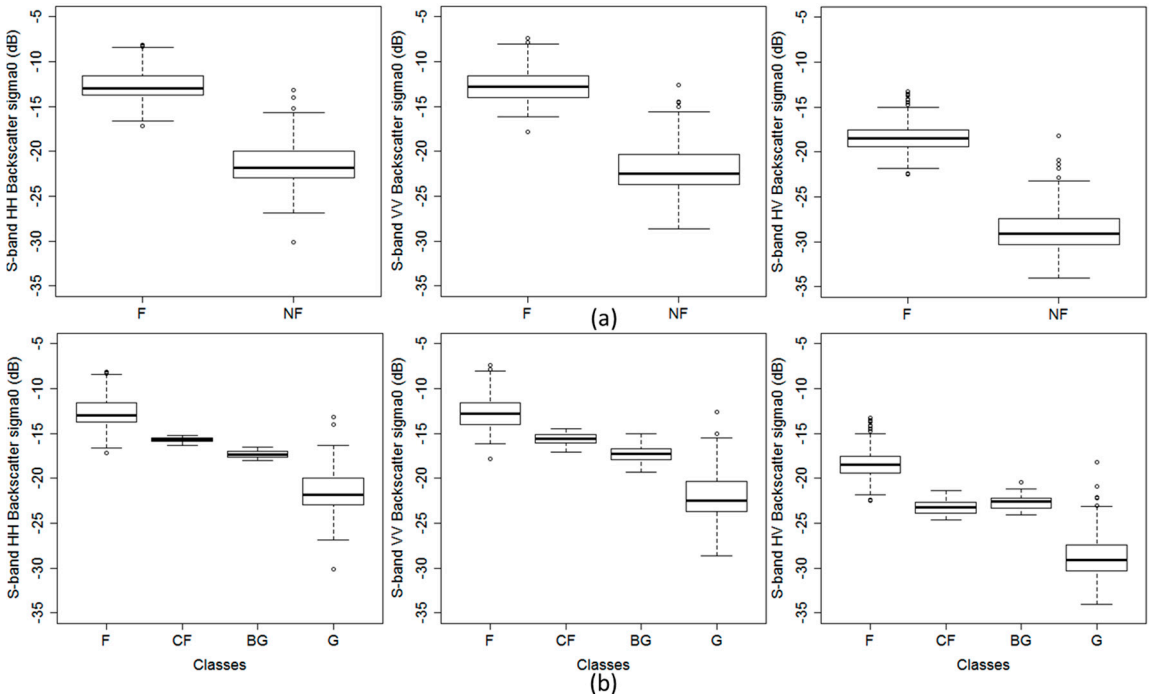


Figure 5. Box-plots of scattering returns from 2014 acquired S-band SAR backscatter in 105 (F–Forest) and 105 (NF–Non-forest) sample plots (**a**) and different non-forest types with 50 (CF–Cleared-felled); 45 (BG–Bare-ground) and 10 (G–Grassland) sample plots; (**b**). The central box in each box plot shows the inter-quartile range and median; whiskers indicate the 10th and 90th percentiles.

Different algorithms have been developed for land cover classification particularly related to forest cover types. Studies have shown that the MLC algorithm can be considered more reliable than other classifier approaches [49]. The algorithm estimates class probability density functions assuming a multivariate normal distribution of the spectral signatures and often achieves better accuracy with SAR data than other classifiers [50].

The changing information content of S-band radar backscatter was examined for different spatial resolutions by re-sampling from the original 0.75 m to different spatial resolutions and repeating the classification. The spatial aggregation was performed for each polarisation band using nearest neighbour resampling with the aid of the Ordnance survey master map. The spatial scales of the forthcoming NovaSAR-S imaging modes of 6 m and 20 m were studied. For the assessment of classification accuracy, 20 non-forest and 21 forest independent points based on the ancient tree database and aerial photos were incorporated along with the training plots, providing 126 forest and 130 non-forest points to provide cross-validation (Figure 1). These sample points were collected at the boundaries of classes (forest to clear-felled, forest to bare-ground, forest to grassland) where mixed pixels with different land cover types exist and are often associated with high error [51]. Therefore, an attempt was made to highlight the accuracies of forest cover and its change maps focusing on the mixed pixels in addition to the homogenous classes. A confusion matrix was computed and the Overall accuracy, User's and Producer's accuracies and Kappa coefficient (κ) were calculated. A cross-comparison with the ALOS PALSAR-based global forest cover map provided by the Japan Aerospace Exploration Agency (JAXA) at 25 m scales was also carried out [52] (Figure 6a,b).

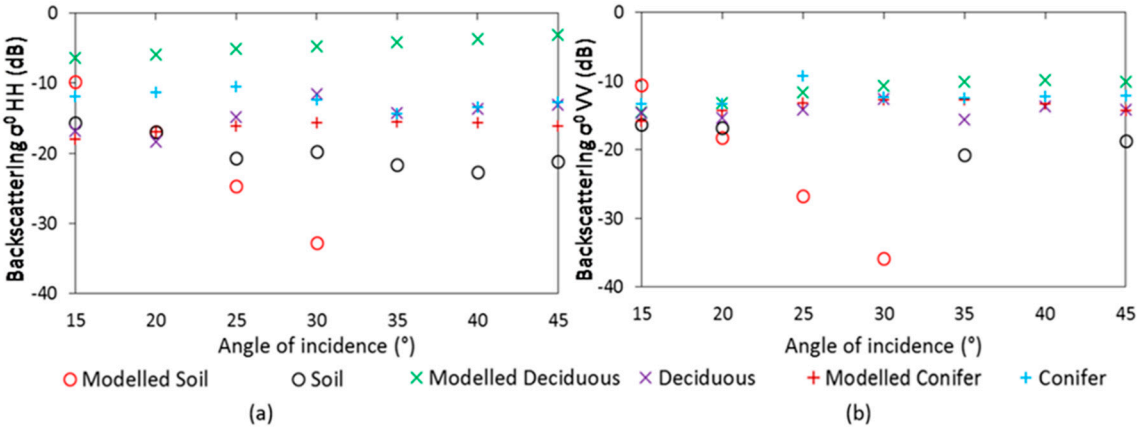


Figure 6. Comparison of observed and simulated forest canopy (deciduous, conifers) and soil total backscatter at S-band frequency for HH (**a**) and VV; (**b**) polarisation.

For forest cover change detection analysis, the classified FNF maps derived from the 2010 and 2014 S-band acquisitions were assessed for changes due to management operations (i.e., clear-felling and thinning) based on a post-classification technique. The Global Forest Watch (2000–2014) product at 30 m based on multi-temporal Landsat data from the global forest change project [53] was also utilized for cross-comparison. Both PALSAR and Landsat-based products are intended to support the interpretation of the S-band derived maps.

3. Results and Discussion

3.1. MIMICS-I Model Simulation Experiment

The forest canopies simulations with MIMICS-I suggest strong S-band radar total backscatter returns particularly in deciduous stands and slightly weaker scattering from coniferous canopies (Figure 6). Total backscatter at HH-polarisation is high due to ground/trunk interactions from the deciduous canopy, higher than for a coniferous canopy. This trend is also evident for VV-polarisation. In all polarisations, backscatter from bare-ground (a function of soil moisture and roughness) is lower across the whole incidence angle range than forest canopy backscatter. This lower backscatter from soil could be due to single scattering from the soil surface. The simulation suggests that S-band backscatter can differentiate forest and non-forest due to the loss of the double-bounce scattering from ground/trunk interaction when the canopy is removed.

In comparison to the model predictions, the observed S-band radar backscatter from the airborne data reveals a similar trend to the model output but with lower sensitivity for both forest types and soil characteristics. These differences could be due to the different levels of branch (primary, secondary) and leaf density assumed in the model. The differences between simulated and observed backscatter from soil could also be due to the single scattering from soil surface as a function of soil parameters assumed in the model with limited field data on soil properties. Additionally, the observed soil backscatter could also have some influence from neighbouring classes (i.e., forest) while extracting the pixel information due to the trade-off between the size of the bare-ground (roads and pathways) and pixel spacing. The radiative scattering mechanisms at S-band simulated by MIMICS-I show a similar behaviour to the longer wavelength at L-band for forested areas [54].

3.2. Forest/Non-Forest Classification Results and Accuracy Assessment

Using the S-band radar backscatter coefficient at HH- and VV-polarisation and the RFDI in the MLC algorithm, a map of F/NF classes over Savernake forest was produced at the NovaSAR-S 6 m and 20 m resolutions (Figure 7). For the 6 m resolution, the forest class is dominant in the Savernake forest area and covers 648 ha. The forest class covers 86% of the classified image, in comparison to 88.26%

based on the FC sub-compartment database. At the spatial resolution of the 20 m resolution case, an over-estimation of the forest class was observed, resulting in an estimated 696 ha of forest (Table 4).

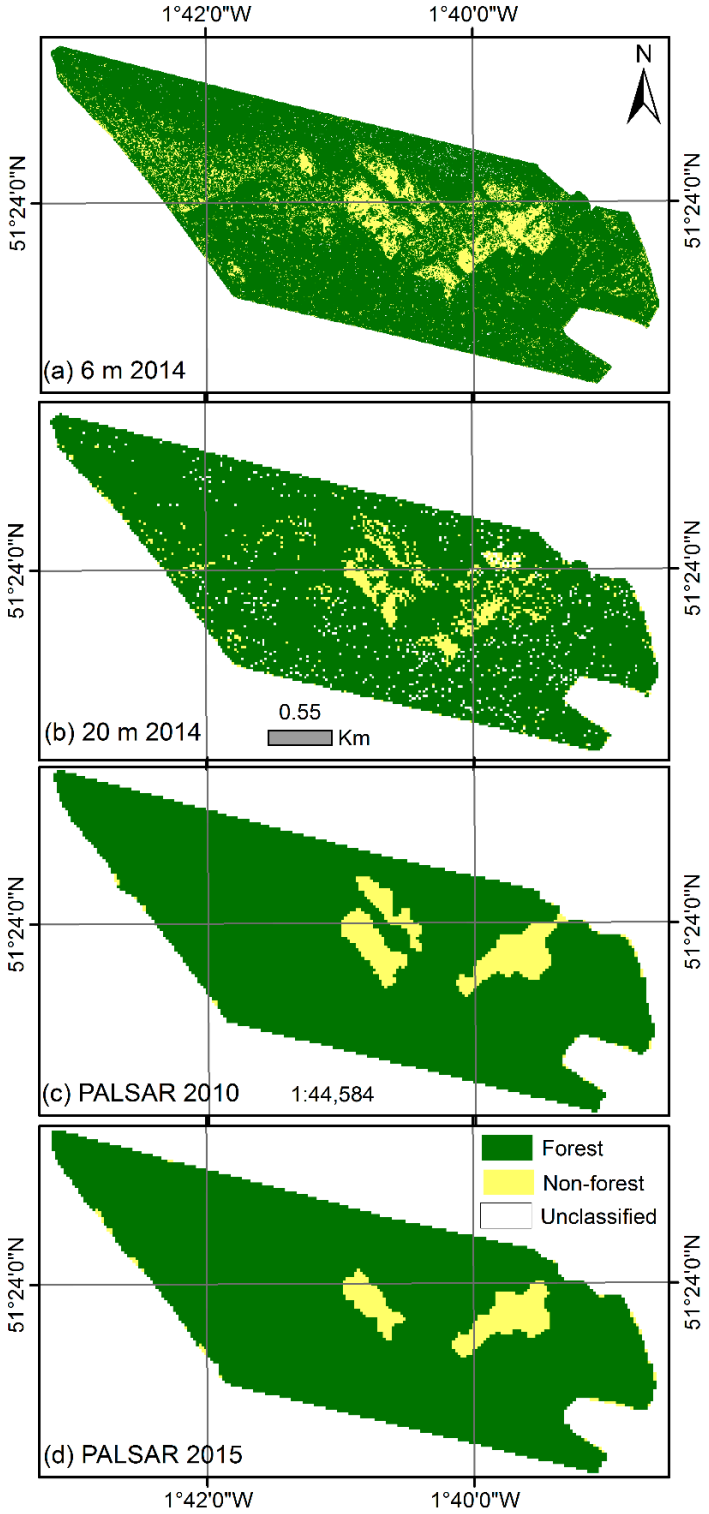


Figure 7. FNF cover map of Savernake using S-band polarimetry and maximum likelihood algorithm at 6 m (**a**) and 20 m (**b**) resolutions and for PALSAR imagery based from 2010 (**c**) and 2015 (**d**).

Table 4. Area distribution of FNF cover for Savernake forest.

Class	6 m Area (ha)	20 m Area (ha)
Forest	648.1	696.5
Non-forest	94.05	48.0
Total (ha)	742.15	744.5

The ability to discriminate forest from non-forest at S-band is due to the strong double-bounce scattering as a function of ground/trunk interaction in forest stands. Similar results have been found in the Baginton site of Southern England using the polarimetric scattering entropy H/average alpha angle α and Pauli's polarimetric decompositions [37]. This strong scattering arises predominantly from deciduous forest species due to the complex structural behaviour in comparison to the homogenous conifers. For coniferous species, a lower volume scattering was observed at S-band frequency due to the high needles and branch densities [35].

In the classified map at 20 m resolution, many non-forested areas are misclassified as forest, possibly due to the inability to capture the finer spatial details of varying surface roughness of the non-forested areas at the coarser spatial scale. The overall accuracy of the classified FNF map at 6 m resolution is 70% (κ = 0.4). Users' accuracy exceeded 70% for the non-forest class but was lower for the forest (65%). The producers' accuracies for forest and non-forest were higher 71% and 68% respectively (Table 5). At the 20 m resolution, the classified FNF map has a lower overall accuracy of 63.67% (κ = 0.27) (Table 6). Reduced users' and producers' accuracies are evident.

Table 5. Confusion matrix for F/NF cover classified map at 6 m resolution for Savernake forest against ancient tree locations and aerial photo. Overall accuracy = 69.9%, Kappa coefficient (κ) = 0.4.

	Predicted Class			
Actual class	F *	NF *	Total	User's Accuracy (%)
F	82	44	126	65.08
NF	33	97	130	74.62
Total	115	141	256	
Producers' Accuracy (%)	71.30	68.79		

* F–Forest, NF–Non-forest.

Table 6. Confusion matrix for F/NF cover classified map at 20 m resolution for Savernake forest against ancient tree locations and aerial photo. Overall accuracy = 63.67%, Kappa coefficient (κ) = 0.27.

	Predicted Class			
Actual class	F *	NF *	Total	Users' Accuracy (%)
F	73	53	126	57.94
NF	40	90	130	69.23
Total	113	143	256	
Producers' Accuracy (%)	64.60	62.94		

* F–Forest, NF–Non-forest.

3.3. Detailed Land Cover Classification Results and Accuracy Assessment

The different backscatter responses in the various non-forest land cover types in the study area provide an opportunity to investigate the sensitivity of S-band backscatter to different non-forested surface types (Figure 8 and Table 7). At 6 m resolution, grassland covers 50 ha of the study site. In general, grass leaves have erect inclination with intermediate soil brightness. The lower backscatter returns from grasses at S-band compared to soil could be due to weaker radar backscatter returns as a result of specular scattering from a smooth surface in comparison to the rougher forest canopies [34,36].

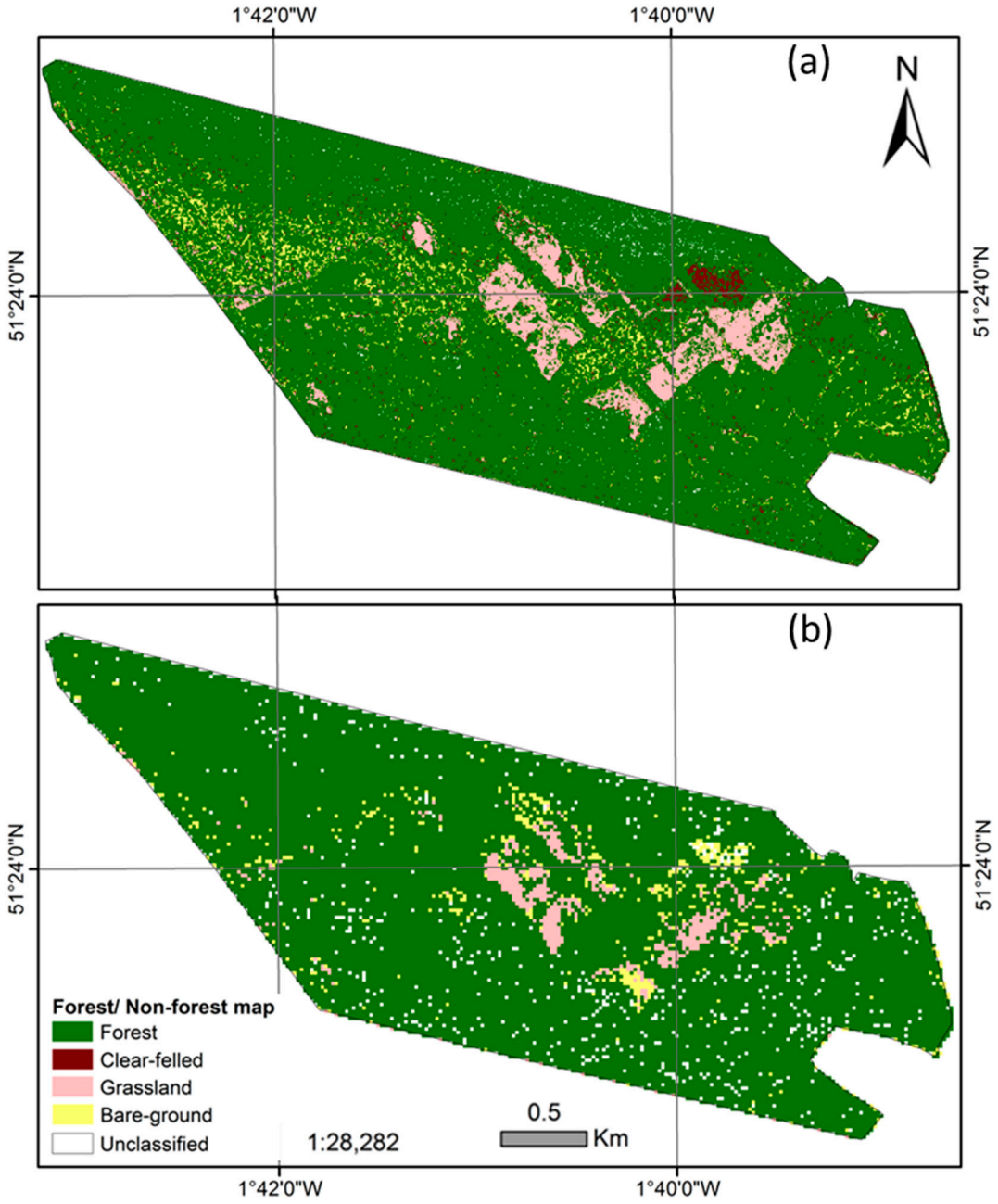


Figure 8. Forest and different non-forest cover map of Savernake using S-band polarimetry and maximum likelihood algorithm at 6 m (**a**) and 20 m; (**b**) resolutions.

Table 7. Area distribution of different non-forest classes for Savernake forest.

Class	6 m Area (ha)	20 m Area (ha)
Forest	648.1	696.5
Clear-felled	13.37	20.36
Grassland	50.33	23.04
Bare-ground	29.88	0
Unclassified	0.47	4.6
Total (ha)	742.15	744.5

Bare-ground and clear-felled areas occupy 29 ha and 13 ha of the classified map at 6 m resolution. The distinctive backscatter signatures of bare-ground and clear-felled areas at 6 m resolution are likely due to the sensitivity of S-band backscatter to surface roughness within these areas. On the basis of the observation data, both bare-ground and clear-felled areas show similar scattering mechanism (Figure 5). Clear-felled areas are often covered with dead leaves and grasses, giving the area a very rough surface after logged operations. The areas in the study site were planted with Norway spruce and oak seedlings, further increasing the surface roughness. In contrast, bare-ground has no vegetation cover and appears as a relatively smooth surface to the radar.

Similarly, the 20 m resolution classification also shows little grassland (23 ha) and bare-ground (20 ha). In this classification map, clear-felled areas were misclassified as bare-ground, possibly due to the different classes being shared as mixed pixels at 20 m resolution which the algorithm could not reasonably map. This is a possible reason for the misclassification of non-forested areas as forest whereas the finer details related to bare-ground and clear-felled were captured by 6 m resolution. The different moisture content of grasses, clear-felled areas and forest classes could be another reason for misclassification because S-band backscatter is also sensitive to moisture content of the soil layer and forest canopies [30]. Closer observation of the classified maps reveals that S-band SAR differentiates forested areas with high backscatter very accurately.

The overall accuracy of the more detailed land cover maps (forest and a variety of different non-forest classes) at both spatial scales revealed a lower overall accuracy than the classified forest/non-forest maps. An overall accuracy of 52.34% (κ = 0.31) for 6 m and 36.72% overall accuracy (κ = 0.07) for 20 m are found (Tables 8 and 9). However, somewhat higher producers' accuracies are observed for all of the non-forest classes at 6 m resolution, particularly for clear-felled areas (71%).

Table 8. Confusion matrix for forest/ clear-felled/grassland/bare-ground cover classified map at 6 m resolution for Savernake forest against ancient tree locations and aerial photo. Overall accuracy = 52.34%, Kappa coefficient (κ) = 0.31.

	Predicted Class					
Actual class	**F ***	**CF ***	**G ***	**BG ***	**Total**	**User's Accuracy (%)**
F	82	7	33	4	126	65.08
CF	16	28	6	0	50	56.00
G	9	1	22	3	35	62.86
BG	8	3	32	2	45	4.44
Total	115	39	93	9	256	
Producer's Accuracy (%)	71.30	71.79	23.66	22.22		

* F–Forest, CF–Clear-felled, G–Grassland, BG–Bare-ground.

Table 9. Confusion matrix for forest/ clear-felled/grassland/bare-ground cover classified map at 20 m resolution for Savernake forest against ancient tree locations and aerial photo. Overall accuracy = 36.72%, Kappa coefficient (κ) = 0.07.

	Predicted Class					
Actual class	**F ***	**CF ***	**G ***	**BG ***	**Total**	**User's Accuracy (%)**
F	73	47	0	6	126	57.94
CF	6	13	25	6	50	26.00
G	5	12	5	13	35	14.29
BG	29	12	1	3	45	6.67
Total	113	84	31	28	256	
Producer's Accuracy (%)	64.60	15.48	16.13	10.71		

* F–Forest, CF–Clear-felled, G—Grassland, BG–Bare-ground.

Closer observation between the F/NF and detailed non-forest classified maps at both 6 m and 20 m resolutions confirms that the spatial resolution influences the discrimination of forested and non-forested areas from S-band backscatter signatures. When the S-band derived F/NF maps at 6 m and 20 m resolutions were compared to the global ALOS PALSAR derived F/NF map for 2010 (at 25 m resolution), a fair agreement between these maps was found. The capacity of the S-band data to detect forest cover is similar to L-band. We now conclude that S-band backscatter can be used to produce forest cover maps, similarly to other wavelengths [22].

This is validated using the global forest cover product of PALSAR at 25 m, though S-band derived maps have lower accuracy level. There is a fair agreement between S-band derived F/NF maps and the PALSAR product. However, the PALSAR forest cover map of 2015 missed out a portion of non-forest (i.e., grassland) while the majority of the forested area is correctly mapped. This may be due to the coarse resolution size of 25 m PALSAR data which missed out in comparison to the airborne datasets. Comparatively, the PALSAR based 2010 data reproduced a combination of both forest and grassland (non-forest) almost similar to the S-band derived 20 m map. This shows that S-band data, similar to L-band data, has a robust capacity to map forest and different non-forest classes as shown above, which may be due to the radiative nature of the S-band backscatter and higher spatial resolution of airborne data. The present findings also support previous results of [36–38].

3.4. Forest Cover Change Analysis

Forest cover change was observed in the S-band backscatter-derived forest cover maps between 2010 and 2014 (Figure 9). Clear-felled areas in two sub-compartments (3.45 ha and 5.2 ha) were confirmed by a field visit in 2015 and the FC database. Thus, clear-felled areas are correctly classified as forest cover change in the FNF map as areas that were NF in 2014 and F in 2010. Figure 9c depicts the change map showing areas undergoing changes from forest to non-forest (red colour) between 2010 and 2014 at 6 m resolution.

A comparison with the forest loss map [53] from 2013 to 2014 from multi-temporal Landsat data at 30 m spatial resolution shows a good correspondence with the forest change between 2010 and 2014 from the S-band SAR (Figure 9d). According to the Landsat-derived forest loss data, the areas of the two clear-cut sub-compartments are 2.3 ha and 4.9 ha. The areas that have changed from forest to non-forest are somewhat different particularly along the class boundaries, where the pixels have mixed cover types (Table 10).

Table 10. Area distribution of FNF cover for Savernake forest between 2010 and 2014 at 6 m resolution.

Class	6 m Area 2010 (%)	6 m Area 2014 (%)
Forest	88	80
Non-forest	12	20
Total (ha)	100	

A small portion of non-forest in 2010 shows a transition to forest in 2014 (Figure 9a,b). This could be a false detection or a plantation that has grown sufficiently to change the radiometric signature at S-band. Previous studies [39,40] highlighted the good capability of S-band SAR in mapping clear-cuts and forested areas in the boreal forest of Canada and Sweden. Based on the results from the temperate forest site at Savernake forest presented here, the S-band SAR backscatter coefficient at all polarisations has shown suitable for monitoring forest cover change but lower than L-band SAR data [21,22]. The S-band SAR sensor on the NovaSAR satellite that is being built in the UK for launch in 2017 will provide image data that can be used for operational forest cover change detection and be used in regions with persistent cloud cover such as the tropics [37,55] and in the boreal winter with low sun angles [39,40].

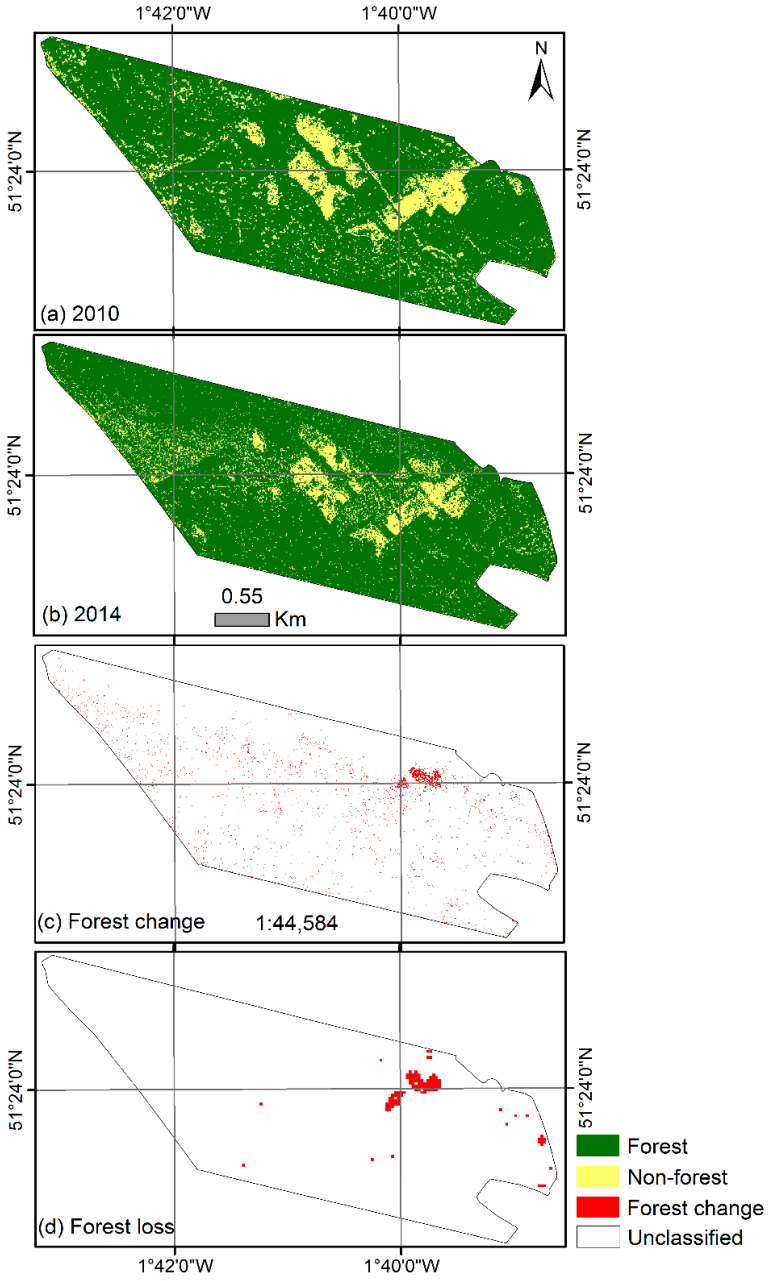


Figure 9. Map results showing S-band derived forest cover at 6 m pixel resolution for 2010 (**a**); 2014 (**b**); detected forest cover change from 2010 to 2014 (**c**) and 30 m resolution Landsat-based forest loss (**d**).

4. Conclusions

High resolution S-band radar data in the context of the AirSAR campaign in Britain was utilised for assessing the mapping of forest/non-forest, different non-forest types and forest cover changes. To assist in identifying the potential of S-band radar backscatter sensitivity to forest canopies, the Michigan Microwave Canopy Scattering (MIMICS-I) radiative transfer model was utilised. This study was conducted in a temperate mixed forest of Savernake forest in England where different species of deciduous and coniferous stand grow. The mapping was conducted in two scenarios: one related to forest/non-forest and the second with different non-forest types (grassland, cleared-felled and bare-ground) that are found in the study area. Using the Maximum likelihood classification algorithm with HH- and VV-polarisation and the Radar Forest Degradation Index

(RFDI) forest/non-forest and different non-forest types were mapped at 6 m and 20 m resolutions corresponding to StripMap and ScanSAR resolution modes of NovaSAR-S.

MIMICS-I model reveals strong S-band backscatter sensitivity to the forest canopy in comparison to soil (bare-ground) across all polarisations and incidence angles. A greater sensitivity of S-band backscatter to the forest canopy was found with a broad-leaved canopy in comparison to coniferous canopy. The overall accuracy of the classification was high reaching up to 70% (κ = 0.41) for 6 m and 63% (κ = 0.27) for 20 m resolution modes. The reduction in accuracy with 20 m resolution map is due to the nature of the MLC algorithm which allocates every pixel to only one class rather than the actual mixed land cover and the size of the signal resolution resulting in mixed pixels [51,56]. This also means that the level of misclassification due to the pixels of multiple land cover classes is a function of spatial resolution. The coarser the spatial resolution, thus the lower is the overall accuracy level. However, such misclassification can be either minimized or improved by adopting an alternative mapping approach based on identifying the membership of each class to the pixel e.g., super-resolution analysis at the sub-pixel scale [57,58]. Additionally, S-band backscatter could also map different non-forest classes with overall accuracy 52% (κ = 0.31) particularly recently clear-felled areas at sub-hectare level (71% producers' accuracy). S-band backscatter between 2010 and 2014 data also found forest cover change detection for sub-compartments having 3–5 ha area due to the loss of the double-bounce scattering from ground/trunk interaction when the canopy is removed. This observation is supported by modelling predictions for deciduous species. Although these results indicate the considerable potential for mapping forest cover and non-forest types using MLC algorithm for S-band SAR backscatter, further research using the alternative classification algorithm is required.

The results show that S-band SAR data from NovaSAR-S could potentially be suitable for mapping forest/non-forest and different non-forest in details and monitor forest cover changes for temperate mixed forest considered in this paper. Current (e.g., Huan Jing-1 Constellation) and future space-borne (e.g., NovaSAR-S and NISAR) S-band SAR missions will continue to provide opportunity to generate forest cover extent including change maps at stand level from continental to global scale. This benefit can be acknowledged as the SAR system can provide continuous data in areas where cloud cover prevents observations from optical sensor data or can be integrated with optical data to provide better detection of forest dynamics such as regeneration, degraded areas and deforestation etc. However, the challenge will be the full integration of SAR data acquired in different frequencies and modes which holds enormous potential to expand on studies related to forest monitoring such as degraded canopy cover and biophysical retrieval.

Acknowledgments: The authors acknowledge the AirSAR data from Airbus Defence and Space, Natural Environment Research Council, Airborne Research & Survey Facility and Space Applications Catapult (Project Code: AS 14/24) to Heiko Balzter, Kevin Tansey, Ramesh K. Ningthoujam, Keith Morrison and Sarah C.M. Johnson, and GIS database from Forestry Commission (Bristol and Savernake, UK). Leland Pierce from the Radiation Lab, The University of Michigan (United States of America) is highly appreciated for providing the MIMICS-I code. Pedro Rodriguez-Veiga, Barnard Spies, Chloe Barnes, James Wheeler, Valentin Louis, Thomas Potter, Marc Padilla (CLCR, University of Leicester) and Alexander Edwards-Smith and Jaime Polo Bermejo (Cranfield University) are acknowledged for assistance in field data collection in 2012 and 2015. Heiko Balzter was supported by the Royal Society Wolfson Research Merit Award, 2011/R3 and the NERC National Centre for Earth Observation.

Author Contributions: This research study was designed and developed by Ramesh K. Ningthoujam, Heiko Balzter and Kevin Tansey in support to NovaSAR future mission applications in forest mapping. Ramesh K. Ningthoujam processed and analysed SAR data (assisted by Geoff Burbidge, Sam Doody, Sarah C.M. Johnson, Nick Veck and Gary M. Llewellyn), field data (assisted by Keith Morrison and Thomas Blythe) and simulated MIMICS-I model predictions (assisted by Kevin Tansey and Heiko Balzter), wrote the manuscript and coordinated revisions. France Gerard and Charles George provided the soil moisture information from Wytham Woods. All authors contributed to the interpretation of the results.

Conflicts of Interest: The authors declare no conflict of interest.

References

1. Foley, J.A.; Kutzbach, J.E.; Coe, M.T.; Levis, S. Feedbacks between climate and boreal forests during the holocene epoch. *Nature* **1994**, *371*, 52–54. [CrossRef]
2. Ciais, P.; Denning, A.S.; Tans, P.P.; Berry, J.A.; Randall, D.A.; Collatz, G.J.; Sellers, P.J.; White, J.W.C.; Trolier, M.; Meijer, H.A.J.; et al. A three-dimensional synthesis study of δ^{18}o in atmospheric co2: 1. Surface fluxes. *J. Geophys. Res.* **1997**, *102*, 5857. [CrossRef]
3. Groombridge, B.; Jenkins, M.D. *World Atlas of Biodiversity*; University of California Press: Berkeley, CA, USA, 2002.
4. Hansen, M.C.; Potapov, P.V.; Moore, R.; Hancher, M.; Turubanova, S.A.; Tyukavina, A.; Thau, D.; Stehman, S.V.; Goetz, S.J.; Loveland, T.R.; et al. High-resolution global maps of 21st-century forest cover change. *Science* **2013**, *342*, 850–853. [CrossRef] [PubMed]
5. Food and Agriculture Organization (FAO). *Global Forest Land-Use Change 1990–2005*; Food and Agriculture Organization of the United Nations: Rome, Italy, 2012.
6. Grainger, A. An evaluation of the fao tropical forest resource assessment, 1990. *Geogr. J.* **1996**, *162*, 73–79. [CrossRef]
7. Food and Agriculture Organization (FAO). *Forest Resource Assessment (fra) 2010*; Food and Agriculture Organization of the United Nations: Rome, Italy, 2012.
8. Cihlar, J. Land cover mapping of large areas from satellites: Status and research priorities. *Int. J. Remote Sens.* **2000**, *21*, 1093–1114. [CrossRef]
9. McRoberts, R.E.; Tomppo, E.O. Remote sensing support for national forest inventories. *Remote Sens. Environ.* **2007**, *110*, 412–419. [CrossRef]
10. Bartholomé, E.; Belward, A.S. A new approach to global land cover mapping from earth observation data. *Int. J. Remote Sens.* **2005**, *26*, 1959–1977. [CrossRef]
11. DeFries, R.S.; Hansen, M.; Townshend, J.R.G.; Sohlberg, R. Global land cover classifications at 8 km spatial resolution: The use of training data derived from landsat imagery in decision tree classifiers. *Int. J. Remote Sens.* **1998**, *19*, 3141–3168. [CrossRef]
12. Friedl, M.A.; Sulla-Menashe, D.; Tan, B.; Schneider, A.; Ramankutty, N.; Sibley, A.; Huang, X. Modis collection 5 global land cover: Algorithm refinements and characterization of new datasets. *Remote Sens. Environ.* **2010**, *114*, 168–182. [CrossRef]
13. Lu, D.; Chen, Q.; Wang, G.; Moran, E.; Batistella, M.; Zhang, M.; Vaglio Laurin, G.; Saah, D. Aboveground forest biomass estimation with landsat and LiDAR data and uncertainty analysis of the estimates. *Int. J. For. Res.* **2012**, *2012*, 16. [CrossRef]
14. Herold, M.; Mayaux, P.; Woodcock, C.E.; Baccini, A.; Schmullius, C. Some challenges in global land cover mapping: An assessment of agreement and accuracy in existing 1 km datasets. *Remote Sens. Environ.* **2008**, *112*, 2538–2556. [CrossRef]
15. Castel, T.; Guerra, F.; Caraglio, Y.; Houllier, F. Retrieval biomass of a large venezuelan pine plantation using JERS-1 SAR data. Analysis of forest structure impact on Radar signature. *Remote Sens. Environ.* **2002**, *79*, 30–41. [CrossRef]
16. Boyd, D.S.; Danson, F.M. Satellite remote sensing of forest resources: Three decades of research development. *Prog. Phys. Geogr.* **2005**, *29*, 1–26. [CrossRef]
17. Billington, C.; Kapos, V.; Edwards, M.; Blyth, S.; Iremonger, S. Estimated Original Forest Cover Map—A First Attempt. World Conservation Monitoring Centre. Available online: http://www.Unep-wcmc.Org/forest/original.Htm (accessed on 17 February 2016).
18. Shvidenko, A.; Barber, C.V.; Persson, R. Forests and woodland systems. Chapter 21. In *Ecosystems and Human Well-Being: Current State and Trends*; Hassan, R., Scholes, R., Ahs, N., Eds.; Island Press: Washington, DC, USA, 2005; pp. 585–621.
19. Pan, Y.; Birdsey, R.A.; Phillips, O.L.; Jackson, R.B. The structure, distribution, and biomass of the world's forests. *Annu. Rev. Ecol. Evol. Syst.* **2013**, *44*, 593–622. [CrossRef]
20. United Nations Environment Programme (UNEP); Food and Agriculture Organization (FAO).; United Nations Forum on Forests (UNFF). *Vital Forest Graphics*; United Nations Environment Programme: Nairobi, Kenya, 2009.

21. Thiel, C.; Drezet, P.; Weise, C.; Quegan, S.; Schmullius, C. Radar remote sensing for the delineation of forest cover maps and the detection of deforestation. *Forestry* **2006**, *79*, 589–597. [CrossRef]
22. Shimada, M.; Itoh, T.; Motohka, T.; Watanabe, M.; Shiraishi, T.; Thapa, R.; Lucas, R. New global forest/non-forest maps from alos PALSAR data (2007–2010). *Remote Sens. Environ.* **2014**, *155*, 13–31. [CrossRef]
23. Simard, M.; Saatchi, S.S.; De Grandi, G.D. The use of decision tree and multiscale texture for classification of JERS-1 SAR data over tropical forest. *IEEE Trans. Geosci. Remote Sens.* **2000**, *38*, 2310–2321. [CrossRef]
24. Saatchi, S.S.; Nelson, B.; Podest, E.; Holt, J. Mapping Land Cover Types in the Amazon Basin Using 1 km JERS-1 Mosaic. *Int. J. Remote Sens.* **2000**, *21*, 1201–1234. [CrossRef]
25. Le Toan, T.; Beaudoin, A.; Riom, J.; Guyon, D. Relating forest biomass to SAR data. *IEEE Trans. Geosci. Remote Sens.* **1992**, *30*, 403–411. [CrossRef]
26. Mermoz, S.; Réjou-Méchain, M.; Villard, L.; Le Toan, T.; Rossi, V.; Gourlet-Fleury, S. Decrease of l-band SAR backscatter with biomass of dense forests. *Remote Sens. Environ.* **2015**, *159*, 307–317. [CrossRef]
27. Brolly, M.; Woodhouse, I.H. Vertical backscatter profile of forests predicted by a macroecological plant model. *Int. J. Remote Sens.* **2013**, *34*, 1026–1040. [CrossRef]
28. Beaudoin, A.; Le Toan, T.; Goze, S.; Nezry, E.; Lopes, A.; Mougin, E.; Hsu, C.C.; Han, H.C.; Kong, J.A.; Shin, R.T. Retrieval of forest biomass from SAR data. *Int. J. Remote Sens.* **1994**, *15*, 2777–2796. [CrossRef]
29. Ulaby, F.T.; Sarabandi, K.; McDonald, K.; Whitt, M.; Dobson, M.C. Michigan microwave canopy scattering model. *Int. J. Remote Sens.* **1990**, *11*, 1223–1253. [CrossRef]
30. Du, J.; Shi, J.; Sun, R. The development of HJ SAR soil moisture retrieval algorithm. *Int. J. Remote Sens.* **2010**, *31*, 3691–3705. [CrossRef]
31. Bird, R.; Whittaker, P.; Stern, B.; Angli, N.; Cohen, M.; Guida, R. NovaSAR-S a low cost approach to SAR applications, synthetic aperture Radar. In Proceedings of the IEEE on Asia-Pacific Conference 2013, Tsukuba, Japan, 23–27 September 2013; pp. 84–87.
32. JPL. Mission to Earth: Nasa-Isro Synthetic Aperture Radar. Available online: http://www.Jpl.Nasa.Gov/missions/nasa-isro-synthetic-aperture-radar-nisar/ (accessed on 15 December 2015).
33. Lopez-Sanchez, J.M.; Ballester-Berman, J.D.; Fortuny-Guasch, J. Indoor wide-band polarimetric measurements on maize plants a study of the differential extinction. *IEEE Trans. Geosci. Remote Sens.* **2006**, *44*, 758–767. [CrossRef]
34. Sun, Q.; Zhang, F.; Shao, Y.; Liu, L.; Wang, G.; Bian, Z.; Li, K. S-band backscattering analysis of wheat using tower-based scatterometer. In Proceedings of the 2012 IEEE International Geoscience and Remote Sensing Symposium, Munich, Germany, 22–27 July 2012; pp. 4621–4624.
35. Lopez-Sanchez, J.M.; Fortuny-Guasch, J.; Cloude, S.R.; Sieber, A.J. Indoor polarimetric Radar measurements on vegetation samples at L, S, C and X band. *J. Electromagn. Waves Appl.* **2000**, *14*, 205–231. [CrossRef]
36. Guida, R.; Natale, A.; Bird, R.; Whittaker, P.; Cohen, M.; Hall, D. Canopy classification with S-band polarimetric SAR data. In Proceedings of the 2012 IEEE International Geoscience and Remote Sensing Symposium, Munich, Germany, 22–27 July 2012; pp. 6535–6538.
37. Natale, A.; Guida, R.; Bird, R.; Whittaker, P.; Hall, D.; Cohen, M. Validation of s-band data performance for future space borne SAR missions. In Proceedings of the European Conference on Synthetic Aperture Radar, Nurnberg, Germany, 23–26 April 2012; pp. 75–78.
38. Van Beijma, S.; Comber, A.; Lamb, A. Random forest classification of salt marsh vegetation habitats using quad-polarimetric airborne SAR, elevation and optical rs data. *Remote Sens. Environ.* **2014**, *149*, 118–129. [CrossRef]
39. Yatabe, S.M.; Leckie, D.G. Clearcut and forest-type discrimination in satellite SAR imagery. *Can. J. Remote Sens.* **1995**, *21*, 455–467. [CrossRef]
40. Fransson, J.E.S.; Walter, F.; Olsson, H. Identification of Clear Felled Areas using SPOT P and Almaz-1 SAR Data. *Int. J. Remote Sens.* **1999**, *20*, 3583–3593. [CrossRef]
41. Crutchley, S.P.; Small, F.; Bowden, M. *Savernake Forest: A Report for the National Mapping Programme*; English Heritage: Swindon, UK, 2009; pp. 1–75.
42. Baker, J.R.; Mitchell, P.L.; Cordey, R.A.; Groom, G.B.; Settle, J.J.; Stileman, M.R. Relationships between physical characteristics and polarimetric Radar backscatter for corsican pine stands in thetford forest, UK. *Int. J. Remote Sens.* **1994**, *15*, 2827–2849. [CrossRef]
43. Airbus. *Airborne SAR Demonstrator Facility (Airsar) Flight Plan*; Airbus Defence and Space: Hampshire, UK, 2013; pp. 1–98.

44. Airbus. *Airborne SAR Demonstrator Facility (Airsar) d2: User Guide*; Airbus Defence and Space: Hampshire, UK, 2013; pp. 1–43.
45. Lu, D.; Mausel, P.; Brondizio, E.; Moran, E. Change detection techniques. *Int. J. Remote Sens.* **2004**, *25*, 2365–2407. [CrossRef]
46. Batjes, N.H. *World Soil Property Estimates for Broad-Scale Modelling (Wise30sec)*; Report 2015/01; Isric—World Soil Information: Wageningen, The Netherlands, 2015.
47. Ulaby, F.T.; Sarabandi, K.; McDonald, K.; Whitt, M.; Dobson, M.C. *Michigan Microwave Canopy Scattering Model (Mimics)*; Report 022486-t-1; University of Michigan Radiation Laboratory: Ann Arbor, MI, USA, 1988.
48. Mitchard, E.T.A.; Saatchi, S.S.; White, L.J.T.; Abernethy, K.A.; Jeffery, K.J.; Lewis, S.L.; Collins, M.; Lefsky, M.A.; Leal, M.E.; Woodhouse, I.H.; et al. Mapping tropical forest biomass with Radar and spaceborne LiDAR in lopé national park, gabon: Overcoming problems of high biomass and persistent cloud. *Biogeosciences* **2012**, *9*, 179–191. [CrossRef]
49. Mather, P.M.; Tso, B.; Koch, M. An evaluation of landsat tm spectral data and SAR-derived textural information for lithological discrimination in the red sea hills, sudan. *Int. J. Remote Sens.* **1998**, *19*, 587–604. [CrossRef]
50. Alberga, V. A study of land cover classification using polarimetric SAR parameters. *Int. J. Remote Sens.* **2007**, *28*, 3851–3870. [CrossRef]
51. Foody, G.M. Status of land cover classification accuracy assessment. *Remote Sens. Environ.* **2002**, *80*, 185–201. [CrossRef]
52. Japan Aerospace Exploration Agency. *New Global 25 m-Resolution Palsar-2/Palsar Mosaic and Global Forest/Non-Forest Map*; Japan Aerospace Exploration Agency: Tsukuba, Japan, 2014.
53. Hansen, M.C.; Potapov, P.V.; Moore, R.; Hancher, M.; Turubanova, S.A.; Tyukavina, A.; Thau, D.; Stehman, S.V.; Goetz, S.J.; Loveland, T.R.; et al. *Global Forest Change 2000–2014*; University of Maryland: College Park, MD, USA, 2014.
54. Grover, K.; Quegan, S.; Freitas, C.D. Quantitative estimation of tropical forest cover by SAR. *IEEE Trans. Geosci. Remote Sens.* **1999**, *37*, 479–490. [CrossRef]
55. Lynch, J.; Maslin, M.; Balzter, H.; Sweeting, M. Choose satellites to monitor deforestation. *Nature* **2013**, *496*, 293–294. [CrossRef] [PubMed]
56. Aplin, P. On scales and dynamics in observing the environment. *Int. J. Remote Sens.* **2006**, *27*, 2123–2140. [CrossRef]
57. Atkinson, P.M. Sub-pixel target mapping from soft-classified, remotely sensed imagery. *Photogramm. Eng. Remote Sens.* **2005**, *71*, 839–846. [CrossRef]
58. Kasetkasem, T.; Arora, M.K.; Varshney, P.K. Super-resolution land cover mapping using a markov random field based approach. *Remote Sens. Environ.* **2005**, *96*, 302–314. [CrossRef]



© 2016 by the authors; licensee MDPI, Basel, Switzerland. This article is an open access article distributed under the terms and conditions of the Creative Commons Attribution (CC-BY) license (http://creativecommons.org/licenses/by/4.0/).



https://dspace.org/

Mapping forest cover and forest cover change with airborne S-band radar

Ningthoujam, Ramesh K.; Tansey, Kevin; Balzter, Heiko; Morrison, Keith; Johnson, Sarah C. M. ...

2016-07-08

http://dspace.lib.cranfield.ac.uk/handle/1826/10173

Ningthoujam RK, Tansey K, Balzter H, et al., (2016) Mapping forest cover and forest cover change with airborne s-band radar. Remote Sensing, Volume 8, Issue 7, July 2016, Article number 577

Downloaded from a DSpace repository. https://dspace.org/